Engng.J.CMU.(2017) 24 (2), 161-175

วารสารวิศวกรรมศาสตร์
มหาวิทยาลัยเชียงใหม่
Engineering Journal
Chiang Mai University

Performance of Hybrid Fuzzy and Neuro-fuzzy Controller with MOHGA based MPPT for a Solar PV Module on Various Weather Conditions

Rati Wongsathan
Department of Electrical Engineering, Faculty of Engineering, North-Chiang Mai University, Hang Dong, Chiang Mai, Thailand, 50230
E-mail: rati1003@gmail.com, rati@northcm.ac.th, Tel. +66(53)819999, Fax. +66(53)819998

ABSTRACT

This paper presents the integration of fuzzy logic (FL) and neuro-fuzzy (NF) with genetic algorithm (GA) to propose FL controller (FLC-GA) and NF controller (NFC-GA) based on Maximum Power Point Tracking (MPPT) for the solar photovoltaic (PV) module. Multi-Objective Hierarchical GA (MOHGA) is used to extract the fuzzy rules and simultaneously fine-tuned the shape of membership functions and the system parameters. In the simulation, the current-voltage characteristic from the PV equivalent circuit model is formulated from the neural networks estimation model in order to calculate the referenced MPP at various weather conditions. It is shown that the FLC-GA performs the best stabilized accuracy at the steady state over the conventional FLC, the NFC-GA, the conventional incremental conductance (IC) method and the perturb and observe (P&O) method respectively. However, for the case of the time response at the transient state, the NFC-GA performs the fast tracking to the MPP over the conventional FLC, the FLC-GA, the P&O method, and the IC method respectively. Furthermore, the high complex structure of NFC-GA including many system parameters which may lead ineffective controller is optimized through MOHGA. The optimized NFC-GA is considered to perform the best result both transient and steady state except for the existing of the severe overshoot which is not suitable for the practice.

Keywords: Fuzzy logic control, Neuro-fuzzy control, Multi-objective hierarchical genetic algorithm, Photovoltaic module.

I. INTRODUCTION

The electrical power generated by PV changes continuously with the environmental conditions mainly the irradiance (G) and ambient temperature (T) which are disadvantages. To obtain the maximum efficiency of the PV, it is necessary to operate the PV at its maximum power point (MPP) for all environmental conditions. To overcome this problem, the maximum power point tracking (MPPT) technique will be developed and applied in the PV power system. The MPPT control algorithm is usually applied in the DC-DC boost converter which is normally interfaced between PV panel and load. The operating point is converged to the MPP by varying the duty-cycle of the power converter through the control command from the pulse width modulation (PWM) signal. The typical diagram of power control based MPPT of the PV system with the switching interface is shown in Fig.1.

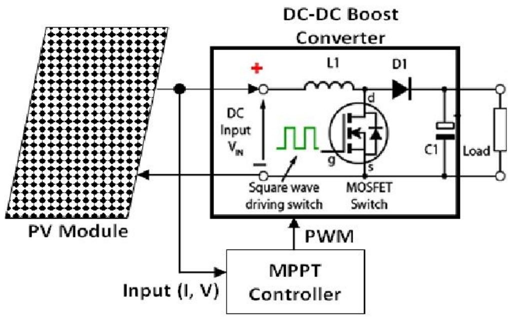

Figure 1 Typical diagram of power control based MPPT of PV system.

Extracting the maximum power output from the PV panel which is available only at one spectific condition, a number of control algorithms based on MPPT are developed in various ways. AI based methods are increasingly popular one, which are adopted in MPPT due to the learning property in interpolation and extrapolation of the non-linear nature of any data

Received 29 June 2016
Accepted 26 January 2017

with high accuracy. Neural Networks (NNs) is a powerful technique for learning the relationship of input-output data but it lacks the heuristic sense and works as a black box [1]. Some of applications of NNs based MPPT in PV are presented in [2]-[4]. On the other hand, FL control (FLC) is implemented without requiring such the big data and sensor. It has the capability of mapping heuristic and linguistic terms of the unknown system into numerical values through the designed fuzzy rules and membership function. It also returns the heuristic output by quantifying the actual numerical data into heuristic and linguistic term [5]. The FLC based MPPT for PV sytem is available in [6]-[7] which have high tracking accuacy under steady state of weather condition but still exhibits some trade-offs between tracking speed and tracking accuracy at the fast change weather condition. The difficult of parameter selection of the membership functions and fuzzy rules is the main criteria which directly rely on the prior knowledge of the system. Recently, it integrates the potential benefits of NNs and FL to form a hybrid system as ANFIS architecture in order to estimate the MPP which is utilized in [8]-[11].

In this work, an increasing of the efficiency on energy conversion of solar PV by static MPPT method through the AI approaches including adaptive fuzzy and neuro-fuzzy controller is our main goal. In order to overcome the parameters and rules selection, the optimization technique as multi-objective hierarchical genetic algorithm (MOHGA) has been introduced to generate the optimized FLC-GA and NFC-GA under the rapidly change weather (i.e. G and T) conditions. To avoid the using of one more controller and without more expensive sensor, the duty cycle is directly generated as the output by account for the derivative of power with respect to voltage or current and its variation as the inputs is also considered here. The comparison performance of both transient and steady state for all proposed controllers with the conventional controllers can be used for decision-making to select the appropriate controller.

The rest of the paper is organized as follows. The overall system configuration including equivalent circuit of PV modeling with its parameters, the I-V and P-V characteristic formulation and the switching device of the interfacing circuit are detailed in section II. Some various controllers are conceptualized to describe the design in step by step procedure presented in section III. Next, the structural design of controllers and their controlled results are shown in section IV with the discussions. Finally, the conclusion is made at the end of the paper in section VI.

II. PV SYSTEM AND INTERFACE

II (A) PV modeling

This section exhibits the solar PV module I-V characteristic obtained from the simulation by Matlab/Simulink. The convenient and most common way in most simulation of PV model is the single diode lumped equivalent circuit model [12] which is composed of 5 parameters i.e. the photo-current (I_{ph}), diode saturation current (I_{sd}), series resistance (R_s), parallel or shunt resistance (R_{sh}), and the ideality factor of diode (n). In order to track the MPP of the PV system by the various control techniques, the accuracy of method depends on the knowledge of these PV parameters which are usually extracted from the experimental data. An equivalent circuit of PV module which is referenced in Fig. 2 and composed of N_s cells in series connection produces the non-linear I_L-V_L characteristic and can be expressed as

$$I_L = I_{ph} - I_{sd}\left(\exp\frac{q\left(V_L/N_S + I_L R_S\right)}{nK_B T} - 1\right) - \left(\frac{V_L/N_S + I_L R_S}{R_{sh}}\right), \qquad (1)$$

where K_B is Boltzmann's constant, q is the electronic charge, and T is the PV temperature in Kelvin. From eq. (1), the parameters of circuit are determined from the I-V characteristic which is preliminarily extracted by the proposed GA.

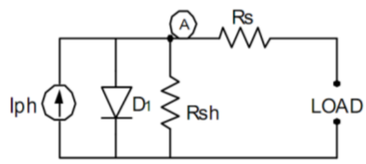

Figure 2 The equivalent circuit with single diode model of the PV module.

In order to describe the influence of weather conditions on these parameters, the translation method was applied by using the parameter translation formula from eq. (2)-(6).

$$I_{ph}(G_2,T_2)=(G_2/G_1)\times\left[1+\alpha(T_2-T_1)\right]I_{ph}(G_1,T_1) \tag{2}$$

$$I_{sd}(G_2,T_2)=(G_2/G_1)\times\left[1+\alpha(T_2-T_1)\right]I_{sd}(G_1,T_1) \tag{3}$$

$$R_s(G_2,T_2)=\frac{\left[1+\beta(T_2-T_1)\right]\left[1+\delta\ln(G_2/G_1)\right]}{(G_2/G_1)\left[1+\alpha(T_2-T_1)\right]}R_s(G_1,T_1) \tag{4}$$

$$R_{sh}(G_2,T_2)=\frac{\left[1+\beta(T_2-T_1)\right]\left[1+\delta\ln(G_2/G_1)\right]}{(G_2/G_1)\left[1+\alpha(T_2-T_1)\right]}R_{sh}(G_1,T_1) \tag{5}$$

$$n(G_2,T_2)=\frac{q(V_L+I_LR_s)}{K_BT}\left[1+\beta(T_2-T_1)\right]\left[1+\delta\ln(G_2/G_1)\right]n(G_1,T_1) \tag{6}$$

The I-V characteristic of the PV module at various weather conditions was finally off-line captured by NNs. While the translation parameters and input variable (voltage and current) will be used as the input of NNs to form the PV module characteristic which is illustrated in Fig. 3. The results were demonstrated through linear variation of short circuit current with G in eq. (7) and variation of open-circuit voltage with T in eq. (8) from condition (G_1,T_1) to (G_2,T_2).

$$I_{sc}(G_2,T_2)=I_{sc}(G_1,T_1)\times\frac{G_2}{G_1}\left[1+\alpha(T_2-T_1)\right], \tag{7}$$

$$V_{oc}(G_2,T_2)=V_{oc}(G_1,T_1)\times\left[1+\beta(T_2-T_1)\right]\times\left[1+\delta\ln\left(\frac{G_2}{G_1}\right)\right], \tag{8}$$

where α and β are the current and voltage temperature coefficients of the test specimen in the standard irradiance for correction and within the temperature range of interest, and δ is a curve correction factor which acts as the temperature coefficient of the internal series resistance. In this work it is resulted that α = -0.048°C^{-1}, β = -0.0194°C^{-1} and δ = 0.06

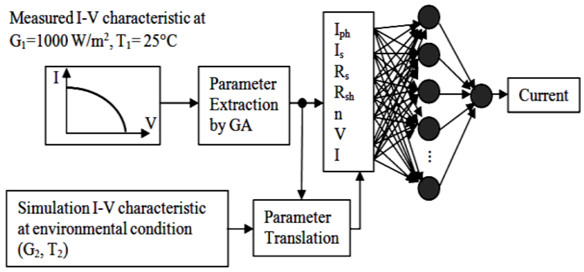

Figure 3 The block diagram of I-V characteristic generation of the PV module at the various weather conditions by the NNs model.

From Fig. 3, the NNs are in simply 3 layers in the structure i.e. input layer with input nodes, hidden layer with N hidden node and nonlinear function commonly hyperbolic tangent function g(.), and an output layer with linearly transfer function f(.). The estimated current (I_{est}) as the output of the NNs is the weighted summation of each hidden layer neuron's output which can be expressed as

$$I_{est}=f\left(b^{(2)}+\sum_{j=1}^{N}w_{j1}^{(2)}\cdot g\left(\sum_{i=1}^{7}w_{ij}^{(1)}PV_i+b_i^{(1)}\right)\right), \tag{9}$$

where $w_{ij}^{(1)}$ are the weight values between input node i^{th} and hidden node j^{th}, $b_i^{(1)}$ are the bias values of input node, $w_{j1}^{(2)}$ are the weight values of hidden node j^{th} and the output node, and $b^{(2)}$ is the bias of output node. PV_i is denoted the input variables which are composed of I_{ph}, I_{sd}, R_s, R_{sh}, n, I and V. The P-V characterized by the hybrid NNs with parameter translation method initiated parameter extraction by GA are shown in Fig. 4 (a)-(b). The MPPs calculated from the simulated I-V characteristeic are used as references of the controlled outcomes from the proposed controllers in section IV.

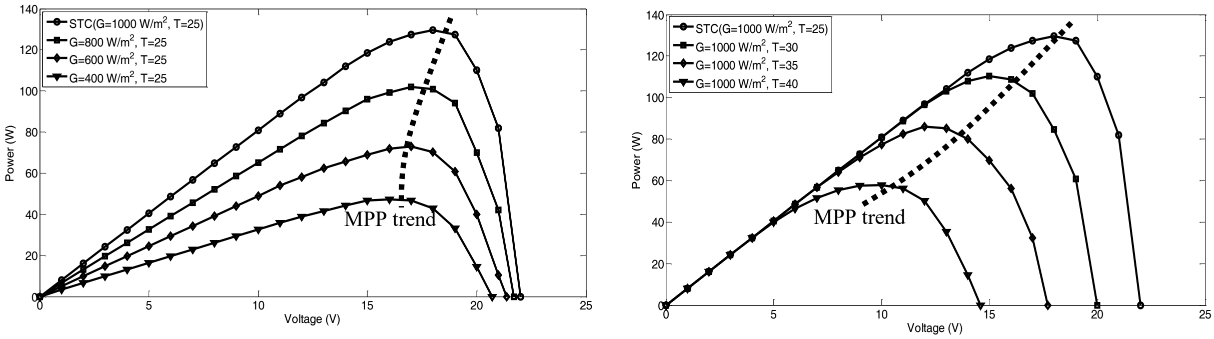

(a) (b)

Figure 4 The *P-V* characteristic of the PV module in the case of (a) varying of the irradiance conditions, and (b) varying of the temperature conditions.

II (B) DC-DC Boost converter

DC-DC boost converter can be used as switching-mode regulator to convert an unregulated dc from PV to a regulated dc output voltage for the load. PWM is normally regulated the voltage and MOSFET or IGBT is used as the switching device. To step up the dc voltage, the DC-DC boost converter is introduced to interface the PV module and the resistive load which was shown in Fig. 1. Through the averaging concept, the input-output voltage relationship for continuous conduction model under steady state is here by given

$$\frac{V_o}{V_{in}} = \frac{1}{1-D} \quad , \tag{10}$$

where D is duty cycle and varies between 0 and 1, thus the output voltage must be higher than the input voltage in magnitude. Similary, the relationship between input impedance (R_{in}) and load impedance (R_{Load}) of a boost converter can be expressed as

$$R_{in} = (1-D)^2 R_{Load} \quad . \tag{11}$$

From eq. (11), it's quite clear that by varying the duty cycle, the input resistance can easily be changed. The increasing duty cycle resulted the decreasing of input impedance, the operation point is moved to the intersection of the load line number 2 and *I-V* curve in Fig. 5. In opposite, the operation point moves to the intersection of the load line number 3 and *I-V* curve. Until duty cycle converges to the optimal, the operation point achieves the MPP at the intersection of load line number 1 and *I-V* curve.

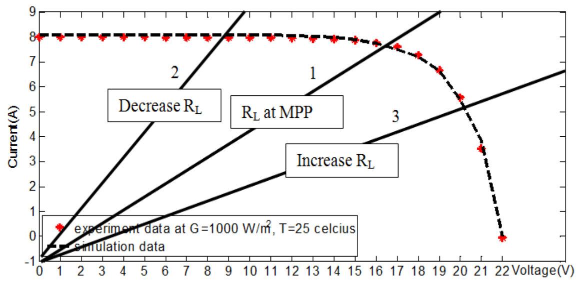

Figure 5 The transition of the operating point location dues to the variation of load impedance.

After filtering the required data from the PV panal (V and I) through A/D module, the differently implemented controller based MPPT schemes will perform to provide the PWM signal for the boost converter in order to generating the controlled duty ratio.

III. CONTROLLER BASED STATIC MPPT TECHNIQUE

The detailed concept and stepwise procedure including of P&O and IC method, the conventional FLC, FLC-GA, and NFC-GA method are described in the sub-section III(A)-(D) respectively.

III (A) Perturb & Observe (P&O) and Incremental conductance (IC) method based MPPT

In this method, the power P_1 corresponds with the instantly measured *I-V* from PV panel is firstly computed to observe the power P_2 after perturbation of a small voltage (ΔV) or duty cycle change (Δd) to the converter in one specific direction. In comparison, if P_2 is more than P_1 then the perturbation is in right direction. Otherwise, the reverse direction is repeatedly done until it met the MPP and also corresponding MPP voltage. The disadvantages of this method are concurrently seen with the experimental results in section IV(A).

To improve the lack of controlled response efficiency from P&O based MPPT under fast varying weather conditions, the incremental conductance or IC method [13] is introduced. This method always adjusts the output voltage according to the MPP voltage based on the incremental and instantaneous conductance (G) of PV module. It exploits the assumption of the ratio of change in output conductor is equal to the negative output conductor at the MPP ($\partial P/\partial V = 0$ while $\partial P/\partial V < 0$ and $\partial P/\partial V > 0$ means the operating point is to the right and left of MPP respectively) or

$$\Delta G = \frac{\Delta I}{\Delta V} = -\frac{I}{V} \quad . \tag{12}$$

If this condition is not met that means $\Delta I/\Delta V > -I/V$ (operating point at the left of MPP) or otherwise, the direction at this operating point must be perturbed until the relationship in eq. (12) succeed. Thus, MPP can be tracked by comparing the instantaneous conductance (I/V) to the incremental conductance (ΔG). It can be determined that the MPPT has reached the MPP and stop perturbing the operating point while P&O method allows the operating point oscillates around the MPP. Although, the IC method is more complicated compared to the P&O method, it can be easily implemented by the advancement of microcontrollers. However, this method requires the accuracy improvement at the steady state [14].

III (B) The conventional fuzzy logic control (FLC) based MPPT

In this work, the slope of PV module's P-V curve, $S(k)$ ($\Delta P/\Delta V$) and the change of slope, $\Delta S(k)$ are used as the fuzzy input variable for E and CE respectively which are defined by eq. (13) and (14) respectively where $P(k)$ and $P(k$-1) is the generated power from PV at time k and k-1 respectively. $S(k)$ can easily be determined the position of the operation point from the MPP which facilitates the increase or decrease of the duty cycle ratio while $\Delta S(k)$ can be used to determine the movement direction of the operating point or the magnitude of the change of duty cycle ratio to prevent fluctuations. The output of the FL is the difference of duty cycle (ΔD) or the duty cycle (D) which are defined by eq. (15) and (16) respectively where FGA is denoted FLC designed parameter by GA,

$$E(k) = \frac{P(k) - P(k-1)}{V(k) - V(k-1)} = \frac{V(k)I(k) - V(k-1)I(k-1)}{V(k) - V(k-1)} \tag{13}$$

$$CE(k) = E(k) - E(k-1) \tag{14}$$

$$\Delta D(k+1) = FGA(\{E(k), CE(k)\}) \tag{15}$$

$$D(k+1) = D(k) + \Delta D(k+1) \tag{16}$$

Typically, there are 3 steps of FLC with includes fuzzification, inference, and defuzzification. Fuzzification step represents the different crisp variable by the predefined fuzzy subsets. In this work, slope of the P-V curve and the change of these slopes are selected as crisp variables. By our consideration, the crisp universe should be partitioned into five different subsets according to 5 regions of P-V curve i.e. left-far from MPP, left-near to MPP, neighbor of MPP, right-near to MPP, and right-far from MPP that generate the total 25 subsets in fuzzy output universe. For partition of crisp universe, the popular Gaussian membership function has been chosen without any selection and representation in eq. (17),

$$\mu_i(x) = \exp\left[-\left(\frac{x - c_i}{\sigma_i} \right)^2 \right] . \tag{17}$$

Where x is the crisp variable, c and σ are the mean and standard deviation of Gaussian function. The degree of membership function (μ) ranging from 0 to 1 of each fuzzy input variable (E and CE) are evaluated for the given crisp input. Then, the rules that contain IF-THEN statements which dictate the statement output are evaluated according to the compositional rule of interference. For example,

Rule 1: **if** E is NB **and** CE is PB **then** D is PB
Rule 2: **if** E is NB **and** CE is NB **then** D is Z

Where NB, PB, and Z is denoted by the negative big, positive big and zero respectively.

In this paper, we used Mamdani's interference typed Max-Min operation which is formulated as,

$$\mu_C(\Delta D) = \max\{\min\{\mu_A(E), \mu_B(CE)\}\} \tag{18}$$

where $\mu_A(E)$, $\mu_B(CE)$, and $\mu_C(\Delta D)$ are the membership value of the membership function of

E, CE and D respectively. After that, defuzzified this fuzzy output into a crisp output using the centre of gravity (COG) method,

$$\Delta D_{COG} = \sum_{j=1}^{n} \Delta D_j \mu_C(\Delta D_j) / \sum_{j=1}^{n} \mu_C(\Delta D_j) \tag{19}$$

where n is the number of fuzzy rules. In this work, the parameters of the membership function of the inputs and output are trial and error tuned and the interference rules have been experienced.

The design experiment results for MF selection between triangular and Gaussian MF with five MFs for input and output variable at the STC are shown in the section IV(B). To build up the FLC based MPPT, a familiar experience of the user on traditional simplified the unknown system through the easily and understandable fuzzy rules. However, the number of fuzzy rules is usually excessive and the topology of the fuzzy sets are inappropriate by this human learning method. Since GA is the powerful searching method for optimal solutions in irregular and high-dimensional solution spaces. Another technique from using GA is adopted to generate the optimized fuzzy model are presented in the next sub-section.

III (C) FLC-GA based MPPT

In this work, GA is also used to optimize the parameters and control rules in FLC based MPPT for rapidly change of weather conditions both irradiance and temperature. However, due to the local minimum trap and slowly convergence to the global solution, GA may be accelerated by the initial solution from the solution of the previously FLC including membership function parameter and user experienced rules. The concept of the FLC based MPPT optimized by GA are shown by the block diagram in Fig. 6.

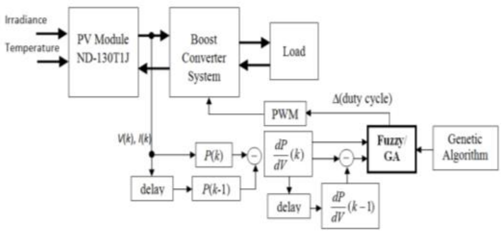

Figure 6 The block diagram of FLC with the parameter tuning by GA (FLC-GA) for MPPT.

The detailed stepwise procedures are described as follow;

Step1: The membership function for 2 inputs (E, ΔE or CE) and one output (D or ΔD) are constructed where each has 5 Gaussian membership functions as Negative Big (NB), Negative Small (NS), Zero (Z), Positive Small (PS), and Positive Big (PB). Each Gaussian function of each membership function has 2 adjusted parameters i.e. mean (C) and standard deviation (σ or W). Then, the total of 3×5×2= 30 parameters and 25 rules are adjusted and selected by GA in the evolution loop.

Step2: Initial population is generated by M_{POP} chromosome. Each chromosome possesses vector entries with certain length of gene which is coded by binary code with the length of N_{bit}. The initial generation index (Gen) is then set to zero. In addition, the speed of GA procedure is accelerated by adding the extra chromosome which is tuned the parameter and designed the rule through human knowledge from the previous result.

Step3: The binary string of each gene is normalized within the range [Q_{min}, Q_{max}] by the linear mapping function as

$$gene(i) = \frac{(Q_{max,i} - Q_{min,i})}{2^{N_{Bit}} - 1} y(i) + Q_{min,i} \quad . \tag{20}$$

Here, $y(i)$ is real value converted from binary string of each gene. In this paper, the parameter c and σ of input E, and ΔE, and output ΔD are normalized within the range [-20, 20], [0.1, 10], [-10, 10], [0.1, 5], [-0.9, 0.9], and [0.01, 0.5] respectively.

Step4: The output, ΔD of each chromosome is computed by the FLC based on MPPT. The PWM is then generated to switch the MOSFET switch of converter. The output voltage at the current operating point moves to the new location according to the I-V characteristic of PV at the given weather condition. The difference between the power at time k ($P_{k,i}$) and reference power (P_{ref}) is cumulatively sum up until the power difference does not change. The totally error, $Error_{k,i}$ is evaluated and scored for ranking chromosome as to their fitness function as,

$$F_i = \frac{M_{POP}}{Err_i(C,W) + 1} , \tag{21}$$

where

$$Err_i(C,W)=\sum_k |P_{ref}-P_{k,i}| \quad . \tag{22}$$

Thus, the higher scoring chromosome has the lower fitness values.

Step5: The parents based on their fitness values are chosen by two methods. First, the elitism method is used to retain the best chromosome that passes through the reproduction step at 10%. Second, the roulette wheel method is used to employ the remaining by assigning a higher probability of selection to individuals with higher fitness values.

Step6: Reproduction by crossover and mutation process with the probability P_C and P_M respectively options to determine how the GAs creates children for the next generation.

Step7: The new generation from step 6 is brought to replace the current population. Steps 2-6 are then repeated in the new generation until convergence is achieved. The algorithm stops if it meets the stopping criterions which are the setting error and maximum iteration.

By the off-line simulation at STC with the setting reference power (P_{ref}) of 130 Watt, MOHGA randomly generates 25 chromosomes (M_{POP}) which are composed of the genes of parameter E, ΔE, and D for shaping the Gaussian function and 25 fuzzy rules corresponding each 5 membership functions of input parameter E and ΔE for simultaneous selecting the fuzzy rules as following;

Chromosome	E	ΔE	ΔD	Rule
Parameter	(C_E,σ_E)	$(C_{\Delta E}, \sigma_{\Delta E})$	$(C_{\Delta D}, \sigma_{\Delta D})$	-
Gene	|1| |10|	|11| |20|	|21| |30|	|31| |55|.

Each gene contains 8 bits of binary (N_{bit}) which are converted to real number for the evaluation. During the GA process, the initial operating point of PV current and voltage are set to 0 A and 0 V which corresponds to 0 W for the initial power. The initial different power (E), different of E (ΔE) and duty cycle ratio are also set to be zero. The individual chromosome takes these initial input variables into the fuzzification step through the MFs which are the Gaussian function with center C_E and $C_{\Delta E}$ and standard variation σ_E and $\sigma_{\Delta E}$. In the rule operation, typically Mamdani inference uses the rules which are in the tail of the chromosome. In the finally FLC step, the defuzzification process defuzzifies the fuzzy output into a crisp output using the centre of gravity (COG) method in eq. (19) through the MFs of parameter ΔD which has center $C_{\Delta D}$ and standard variation $\sigma_{\Delta D}$. The new operating point (V, I) is generated with simultaneously the calculated power. In this work, accounting for the speed of the convergence to the reference power, the resulted power at each sampling time, kT of individual chromosome $P_{k,i}$ are recorded and compared with the P_{ref} to produce the residual following by eq. (22). The ranking of chromosomes are followed the fitness function in eq. (21). The best chromosomes are saved by 10% of the total chromosome through the elitism strategy and the remaining chromosomes are passed through the mutation, crossover and selecting step. Until the stopping criterions are achieved, the best chromosome is chosen and tested on various weather conditions.

III (D) NFC-GA based MPPT

The neuro-fuzzy system typically integrates the powerful learning of NNs and the high interpretability and computational efficiency by using reasoning rules of FL, thus this implies the most potential AI technique. In this work, neuro-fuzzy architecture like the ANFIS model performs as the controller-based MPPT directly generates the change of duty cycle based on the input including E and CE as defined in eq. (13) and (14). Unlike in researches [15]-[17], the MPP is previously generated from ANFIS model which uses the inputs from the weather conditions e.g. G and T then it was applied with another controllers to generate the duty cycle. More sensors are need twice from FLC which are not suitable for the small standalone PV system. The structure of the ANFIS controller based on MPPT is shown in Fig. 7. The first order Sugeno or Takagi-Sugeno-Kang inference [18] was used for ANFIS which is different from Madani inference, while in the Sugeno outputs are linearly a combination of inputs instead of defuzzification method. Sugeno-type FIS has more advantages than the Mamdani because it avoids the use of time consuming in defuzzification process since it is a more compact and computationally efficient representation. It also works well with optimization and adaptive techniques. Moreover it guarantees continuity of the output surface, and is well-suited to mathematical analysis. An example rule with the two fuzzy if-then rules can be expressed as:

If E is PB **and** CE is Z

then $\Delta D = p_1E + q_1CE + r_1$,

where {NB, NS, Z, PS, PB} is fuzzy set in the antecedent and $\Delta D = f(E, CE)$ is a crisp function in the consequent part.

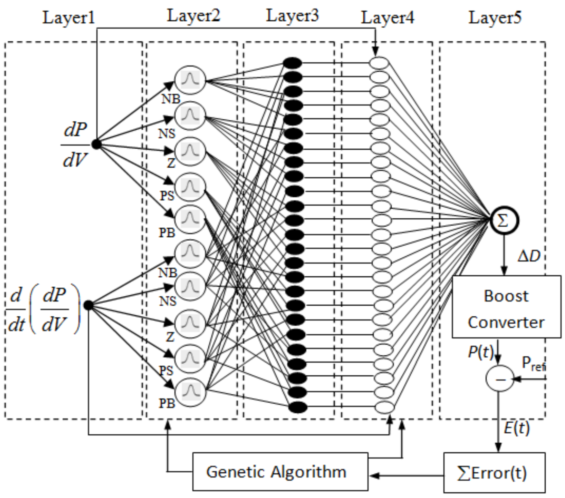

Figure 7 The diagram of NFC (ANFIS) based MPPT.

Generally, the fuzzy rules which are obtained from the clustering or the grid partition based method are updated by NNs which uses back propagation learning method with gradient descent algorithm. Consequently, the premise parameters of the membership function (C_i, σ_i) are also optimized. While the consequently parameters: p_i, q_i, and r_i are designed by least mean square (LMS) method. [19]. In this work, all of parameters are simultaneously selected by GA to avoid a local optimal trapping by the derivative method.

The significant ANFIS based MPPT structure is detailed following:

Layer1: Each input node gives the crisp value to overall membership function in the fuzzy set.

Layer2: Each adaptive node generates the strength of membership function, $O_i^1 \in [0,1]$ for the input vectors. In this paper, the activation function is also Gaussian function which is represented in eq. (17).

Layer3: The total number of rules from the product of membership function of set E and CE are 25 rules. Every node calculates the firing strength according to the rules via a multiplication,

$$O_i^2 = w_i = \mu_{1i}(E)\mu_{2i}(CE),\ i = 1,...,5 \tag{20}$$

Layer4: The strength of rule of each node in this layer has an averaging weight as

$$O_i^3 = \bar{w}_i = \frac{w_i}{\sum_{j=1}^{n} w_j} \tag{21}$$

Layer5: Adaptive node i in this layer computes the contribution of i-th rule towards the overall output, with the following node function, $O_i^4 = \bar{w}_i \Delta D_i$. Then overall output as the summation of contribution from each rule is finally computed as,

$$O_i^5 = \sum_{i=1}^{2} \bar{w}_i \Delta D_i \tag{22}$$

The individual chromosome composed of three genes or variables including error (E), change of error (CE), and consequent parameter.

By the off-line simulation at STC with the setting reference power (P_{ref}) of 130 Watt, MOHGA randomly generates 25 chromosomes (M_{POP}) which are composed of the genes of parameter E and ΔE for shaping the Gaussian function, consequence parameters p, q, and r and 25 fuzzy rule corresponding each 5 membership functions of input parameter E and ΔE for simultaneous selecting the fuzzy rules. The trained parameters from 2×5×2 premise parameters and 5×5×3 consequent parameters are selected by GA with the chromosome representation as following;

Chromosome	E	ΔE	consequent parameter
Parameter	(C_E, σ_E)	$(C_{\Delta E}, \sigma_{\Delta E})$	p,q,r
Gene	|1|, … ,|10|	|11| , … , |20|	|21| , … , |95|

The procedure of MOHGA for NFC is the similar step in section III(C) for FLC except for replacing Mamdani inference by Takagi-Sugeno-Kang inference.

IV. RESULTS AND DISCUSSION

In this section, the performance of the proposed controllers for both transient and steady state with the various weather conditions are investigated and made the comparison among them. The weather conditions are set up in Fig. 8 by varying of the solar irradiance and temperature in the range 600-1000 W/m^2 and 25-40°C respectively. At the initial condition, the weather is set up at STC and rapidly change to low irradiance and high temperature at $kT = 50$. The rest weather condition is set to test the tracking performance of the controllers. The controlled results for individual scheme are described and discussed in next sub-section accordingly.

IV (A) Power control effect from P&O and IC method

The controlled results of the conventional P&O method are represented in Fig. 9. The convergence at the steady state is achieved for the properly step size selection of ΔD with value of 0.02. However, the wide range of the rise time and oscillation still need more and more improvement.

The simulation results under the same weather condition as represented in Fig. 8 by IC method is shown in Fig. 10 for the high perturbation step size equal to 0.05 in order to the fast response. The rise time and oscillation are less in comparison with P&O method. However, the fluctuation and accuracy of MPP at the steady state need more improvement. Further, requiring the complex and costly controlled circuits of this method has disadvantages with respect to P&O method. The tracking time performance for both P&O and IC methods at the faster change weather conditions are quite well since they take a low rise time but the accuracy and fluctuation becomes clearly worse at the steady state. To overcome such the problems, our proposed FLC and NFC are implemented to assist the conventional controllers to obtain the MPP faster and more stable PV output power.

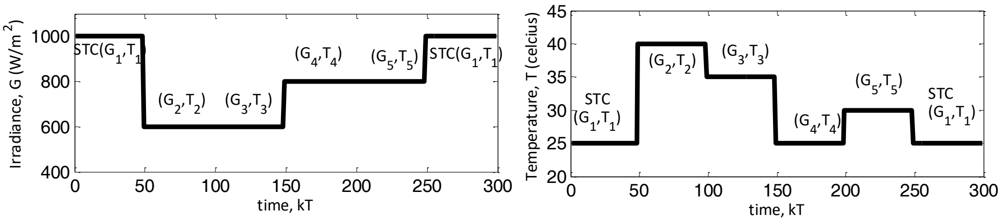

Figure 8 The various of solar irradiance and temperature conditions for the testing of controller based on MPPT.

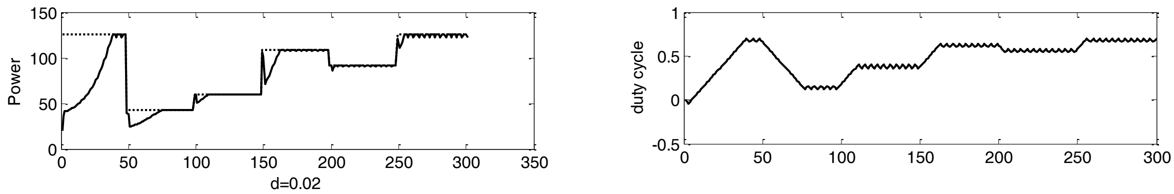

Figure 9 The controlled results from P&O controller with fixed duty cycle method based on MPPT.

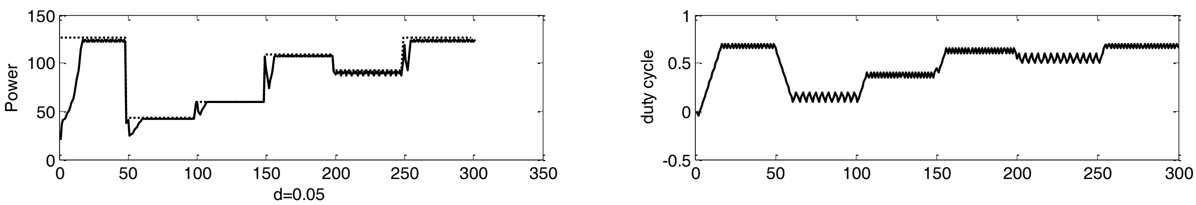

Figure 10 The control result of the IC controller based MPPT.

IV (B) Power control effect of the conventional FLC and FLC-GA

The results of the MFs of the inputs and outputs in both triangle and the Gaussian MF from the design of previous section III(B) for conventional FLC are shown in Fig. 11 (a) and (b) respectively. It was noticed that the membership functions of the duty cycle was not distributed evenly along the universe of discourse (UOD). They were designed for more dense in the range [-0.2, 0.2] which was a sensitively worked zone to achieve near the MPP.

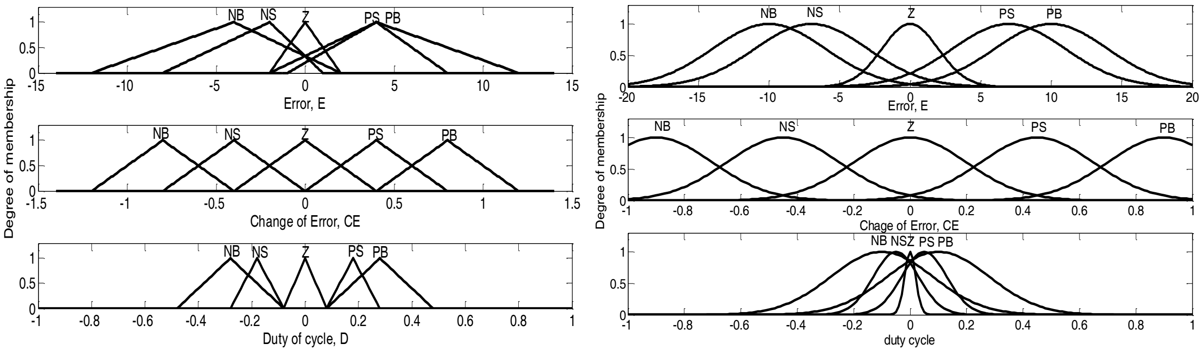

(a) (b)

Figure 11 The designed MFs of the input E and CE and the output ΔD (a) Triangular functions and (b) Gaussian functions, for the conventional FLC.

The fuzzy rules are designed to incorporate the following and to keep in view of the overall control performance

- For the case of the slope of P-V curve or $S(k)$ is NB and $\Delta S(k)$ is Z means the operation point of the PV module is located at the right side and near the MPP, then the duty cycle ratio needs to increase following eq. (10) for decreasing the input impedance in order to shift the operating point to the MPP at the left side. The controlled output is then set to PS to suppress the change of magnitude of the duty ratio in the opposite direction. However, when $\Delta S(k)$ is NB or NS which means the direction towards to the right side then the output control would be set to Z in order to prevent the operating point shift to the left side of the MPP and oscillation. For the case of $\Delta S(k)$ is PS or PB, the output control would be set as NS or NB for increasing the duty cycle ratio in order to shift the operating point to the left according to the movement direction. When $S(k)$ is NS and $\Delta S(k)$ is either negative or zero or positive, the duty cycle ratio under this condition was set in the similar way.

- For the case of $S(k)$ is PB and $\Delta S(k)$ is Z, this means that the operating point of the PV module is located at the left side and near of the MPP, then the duty cycle ratio needs to be decrease following eq. (10) for increasing the input impedance in order to shift the operating point to the MPP at the right side. When $\Delta S(k)$ is also PB or PS, the controller may generate the wrong outputs owing the reason similar to the above mentioned then the controlled output would be set as Z. When $\Delta S(k)$ is NB or NS, the operating point would be set to increase the duty cycle ratio. Then the output control would use PB or PS respectively. When $S(k)$ is PS and $\Delta S(k)$ is either negative or zero or positive, the duty cycle ratio under this condition was set in the similar way.

- For the case of $S(k)$ is Z and $\Delta S(k)$ is Z, the controlled output would be set Z. When $\Delta S(k)$ is NB or NS the controlled output would be set to PB or PS respectively and when $\Delta S(k)$ is PB or PS the controlled output would be set to NB or NS respectively.

Taking this reason into consideration, the fuzzy rules are derived and the corresponding rule based on 25 rules for both triangular and Gaussian MFs are given in Table 1. The effect of the power control by the conventional FLC using triangular MFs for the input and output variables with the same weather conditions test used in P&O and IC method are shown in Fig. 12 for the various change of weather conditions represented in Fig. 9. It is seen that at the lower irradiance and high temperature (at kT = 50) the tracking performance is failed from achieving the MPP target.

Comparing with the conventional FLC using the Gaussian MFs in Fig. 13, it can be seen that the tracking performance of the latter case is better than the former one. At the low irradiance and high temperature condition (kT=50), the tracking had successfully reaches near to a steady MPP at about kT equal to 85. The accuracy on the MPP and the fluctuation at the steady state are minor improvement compared to the conventional methods. This is due to the ability of automatically reducing perturbed voltage after the MPP is identified unlike to the conventional method that is still performing the same size of the perturbed voltage. However, the high rise time at the transient state and the oscillation and accuracy at the steady state need to consequently develop as seen obviously in Fig. 13(a).

Table 1 Fuzzy rule base designed by user experience of FL based MPPT

		E				
		NB	**NS**	**Z**	**PS**	**PB**
	NB	Z	Z	PB	PB	PB
	NS	Z	Z	PS	PS	PS
CE	**Z**	PS	Z	Z	Z	NS
	PS	NS	NS	NS	Z	Z
	PB	NB	NB	NB	Z	Z

Right side of MPP — Near MPP — Left side of MPP

To achieve more good controlled result, the shape of Gaussian MFs and the rule are designed and selected by GA. After all computations are performed, the best shape of five Gaussian MFs of the inputs and output are shown in Fig. 14, the selected fuzzy rules are shown in **Table 2** and the controlled results of FLC-GA are shown in Fig.15.

The NS and PS of output MF are located the same centre like the Z MF. The UOD of the output Gaussian MFs are still dense in the range of [-0.2, 0.2] but a little shifting to the left hand side of the zero in spite of symmetry around the zero. It showed that more reduced step size of perturbed voltage was desired to achieve the MPP. The rule base has differently changed from the previously design by the user. The rule action near the MPP by using the antecedent part from *E* is Z and ΔE is Z is replaced by *E* is PS and ΔE is NS with the same consequent part of *D* is also zero.

Table 2 The designed fuzzy rule base of FLC-GA.

		E				
		NB	**NS**	**Z**	**PS**	**PB**
	NB	Z	Z	PB	PB	PB
	NS	Z	PS	PS	PS	PB
CE	**Z**	PS	NS	Z	Z	Z
	PS	NS	NB	NS	NS	Z
	PB	NB	NB	NS	NS	Z

It can be seen that the FLC-GA performs the better of stabilized accuracy at the steady state than the conventional FLC, IC and P&O method approximately 23.8%, 61.0%, and 61.8% respectively. However, the controlled results from the FLC-GA at the rapidly change condition (i.e especially kT= 50 and 150) has the worsen rise time which is higher than the conventional FLC approximately 79.3% and lower than P&O and IC approximately 36.9% and 41.7% respectively. At first the overshoot has also firstly appeared through this control method. To improve the accuracy together with the preserve the fast transient response, another proposed controller by using NFC is investigated in the next sub-section in order to challenge the trade-off between fast transient response and accuracy at the steady state.

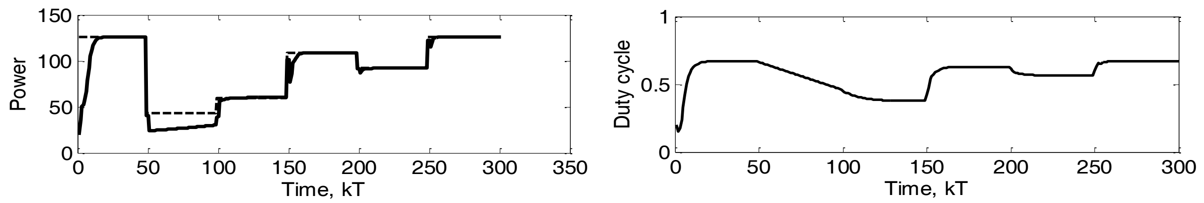

Figure 12 The control results of the conventional FLC for the triangular MF based MPPT.

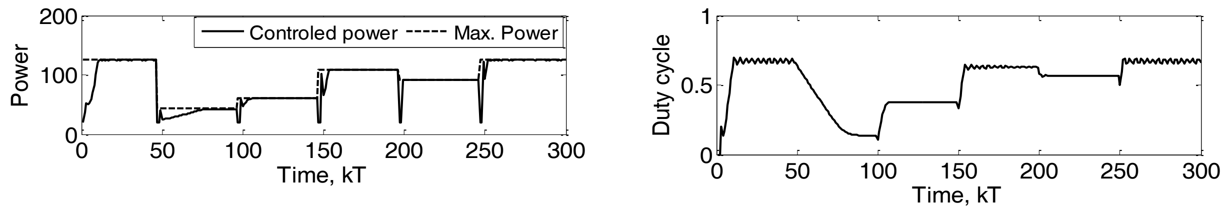

(a) the power tracking for the fast change of weather conditions (b) variation of duty cycle ratio

Figure 13 The control results of the conventional FLC by using the Guassian MFs based MPPT.

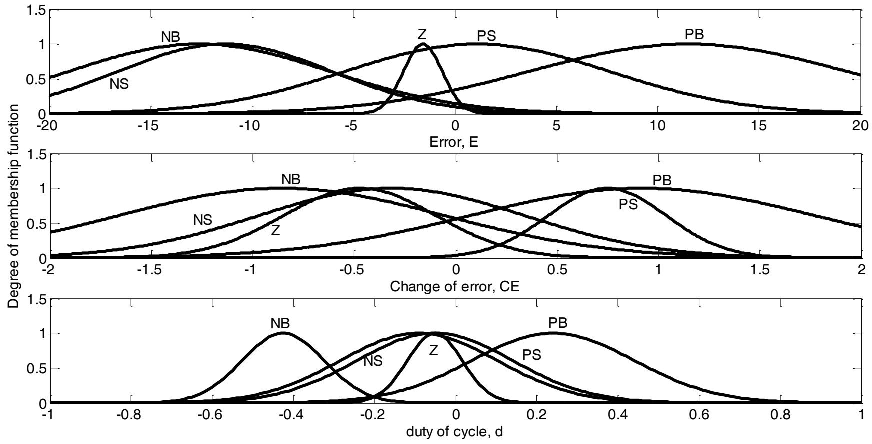

Figure 14 The shape of Gaussian MFs of the input variable *E* and *CE* and the output variable *D* which are selected by GA for FLC-GA based MPPT.

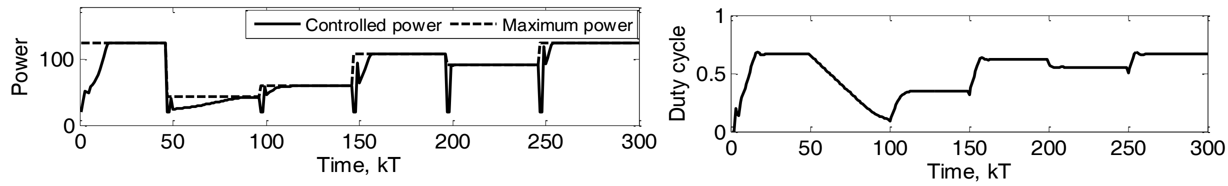

(a) the power tracking for the fast change of weather conditions (b) variation of duty cycle ratio

Figure 15 The control results of the proposed FLC-GA controller based MPPT.

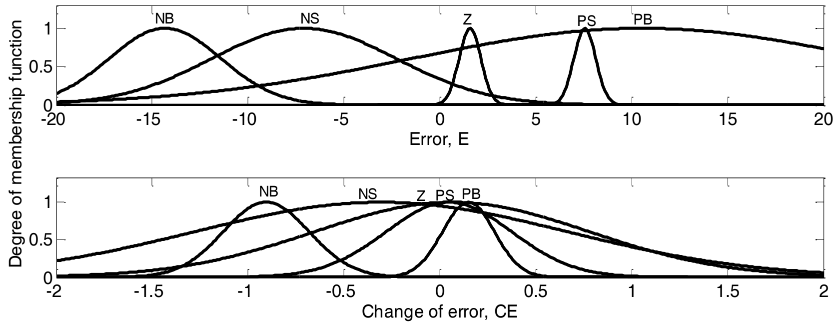

Figure 16 The best shape of MFs and their parameters which are searched by GA method for the input variable *E* and *CE* of the NFC-GA based MPPT.

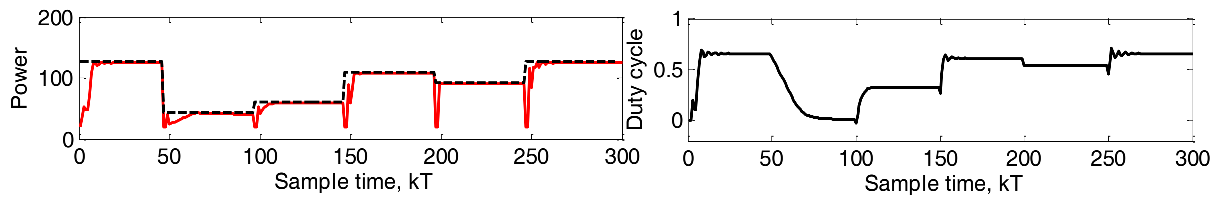

(a) the power tracking for the fast change of weather conditions (b) variation of duty cycle ratio

Figure 17 The control results of NFC-GA based MPPT.

IV (C) Power control effect of NFC-GA

From the designed NFC by GA procedure in section III(D), the best shape MFs of the inputs *E* and *CE* are shown in Fig. 16 and all 20 premise parameters and 75 consequent parameters are also obtained but are not shown here. The controlled results from our proposed NFC-GA are shown in Fig. 17 where the system parameters were designed by GA under the weather conditions represented in Fig. 8. In comparison, our proposed NFC-GA performed the rise time for the rapidly change weather condition less than the conventional FLC, FLC-GA, P&O, and IC respectively. With regards to accuracy of MPP at the steady state by this method is less accurate than the FLC-GA and the user designed FLC but more accurate than IC and P&O. However, the overshoot has severely occurred at the transient state.

The controlled performance at the transient and steady state covers the overshoot, the rise time, the stability and the accuracy. The overall results of the performance at the transient and steady state from all controller schemes obtained from the simulated testing are comparatively shown in **Table 3** which has its own advantages and disadvantages with respect of each controller.

Table 3 Comparison performance of the controllers based MPPT in the case of fast change weather conditions

Controller	Transient state		Steady state	
	Overshoot	Rise time	Oscillation	Accuracy
Conventional P&O	None	Medium	High	Low
Conventional IC	None	Low	High	Low
Conventional FLC	None	Medium	Medium	Medium
FLC-GA	Low	High	None	Very High
NFC-GA (ANFIS)	High	Low	None	High

From the results, it is found that the FLC-GA performs the best accuracy with closely track nearly the MPP over NFC-GA, the conventional FLC, IC and P&O by about 4.95%, 5.58%, 6.10%, and 6.32% respectively while for the case of time response, the NFC-GA performs the MPP fast tracking over the conventional FLC, FLC-GA, P&O, and IC by about 8.75%, 42.27%, 67.05%, and 72.50% respectively.

However, all the self-generated rules do not contribute enough for an accurate improvement while increasing the computation time. In this work, the redundant rules of ANFIS model are further removed by MOHGA while maintains the accuracy in acceptable. The ANFIS controller in the previous section is taken by rule reduction and simultaneously adjusting the parameter of the Gaussian function and consequence parameter of the significant rule. The significances of the proposed ANFIS structure including with the inference type are similarly with the previous one. GA is also used to optimize the system parameters simultaneously reduce the redundant rules. The 25 rules set is randomly generated in binary code which is '0' means not consideration the accordingly rule while '1' means takes the rule into account for calculation. The chromosome represents as following:

Chromosome	E	ΔE	consequence parameters	Rule
Parameter	(C_E, σ_E)	$(C_{\Delta E}, \sigma_{\Delta E})$	p,q,r	{0,1}
Gene	|1|,…,|10|11| ,…, |20|21|	,…,		|45|46|… |70|

After the design of optimized NFC by MOHGA procedure, the number of rules is reduced by 10 rules. The remaining parameters of this ANFIS model are totally 65 parameters which are reduced by 30 parameters from the original ANFIS model. All parameters are also obtained but not shown here. The controlled results by applying the optimized NFC-GA are shown in Fig. 18. It is found that the rise time from the optimized NFC-GA is lower than the NFC-GA about 15% by average but more oscillation and overshoot occurs in the transient state. However, the accuracy at the steady state from the optimized NFC-GA is lower than the NFC-GA about 2.14% by average.

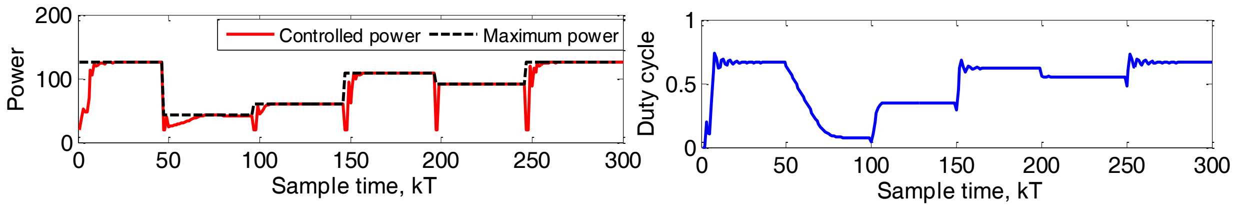

(a) the power tracking for the fast change of weather conditions (b) variation of duty cycle ratio

Figure 18 The control results of the optimized NFC-GA based MPPT.

V. ACKNOWLEDGEMENT

The authors directly acknowledge the research fund support from the research institute of the North-Chiang Mai University. In addition, I'd like to thank to the participate team for setting and measuring the PV module with interfacing.

VI. CONCLUSION

This paper implements the fuzzy logic controller (FLC) and neuro-fuzzy controller (NFC) or ANFIS structure based on maximum power point tracking (MPPT) for a solar photovoltaic module. The proposed FLC and NFC are intentionally implemented to improve the controlled performance of P&O, IC and conventional FLC controller. The design and selection of the system parameters including to the controlled rules of the FLC and NFC are properly selected and tuned by MOHGA and denoted FLC-GA and NFC-GA respectively. In order to test the performance of the proposed controllers, the simulation and testing results were performed on Matlab/Simulink program before the practical implementation. In our experiment, a polycrystalline silicon commercial (SHARP type ND-130T1J) with 36 cells in connected series was adopted for the study. The PV module parameters of the single diode equivalent circuit model are extracted by using the NNs model together with GA and the parameter translation functions in order to generate the *I-V* and *P-V* characteristic under the various weather conditions of both irradiance and temperature. This solar PV module is connected to a resistive load with interfacing by the DC-DC boost converter. The directly measured current and voltage from the panel are used to calculate the slope of *P-V* and its change as the input for all controllers and the duty cycle is generated for the output. The controlled performance at the transient and steady state covers the overshoot, the rise time, the stability and the accuracy. The FLC-GA is dominant on the stabilized accuracy at the steady state while the NFC-GA based ANFIS structure has successful fast tracks to the optimal.

However, the highly complex and computation of the NFC-GA controller may lead the over-fitting and result to miss the optimal power. It should be optimized to reduce the redundant rules and parameters to increase their efficiency. The optimized NFC-GA based ANFIS structure is considered to perform the best result both transient and steady state except for the existing of the severe overshoot which is not suitable for the practice.

Alternately in the future, the NFC may be utilized the weather condition such as irradiance and temperature as the inputs to estimate the MPP instead of using the NNs model which used the number of data to train the network. Furthermore, the other optimizations such as the particle swarm optimization (PSO), artificial bee colony (ABC), etc. are used to optimize the FLC and NFC for alternative searching strategy.

REFERENCES

[1] Haykin, S. Neural network-A comprehensive foundation. 2nd edition, New York Practice Hall Inc., 1999.

[2] Hiyama, T. and Kitabayashi, K. Neural network based estimation of maximum power point generation from PV module using enviromental information. *IEEE Transactions on Energy Conversion*, 1997; 12(3): 241-247.

[3] AI-Amoudi, A. and Zhang, L. Application of Radial Basis Function networks for solar-array modelling and maximum power-point prediction. IEE Proceeding Generation, Transmission and Distribution, 2000; 147(5) 310-316.

[4] Premrudeepreechachan, S. and Patanapirom, N. Solar-array modeling and maximum power point tracking using neural networks. IEEE Bologna Power Tech Conference Proceedings, 2003.

[5] Chen, G. and Pham, T.T. Introduction to fuzzy sets, fuzzy logic, and fuzzy control systems. *CRC Press*, 2000.

[6] Kaisar, M.S., Anwer, A., Aditya, S.K. and Mazumder, R.K. Design and simulation of fuzzy based MPPT. *Renewable Energy Prospect and Progress*, 2005; 19-21.

[7] Kottas, T.L., Boutalis, Y.S. and Karlis, A.D. New maximum power point tracker for PV array using Fuzzy controller in closed cooperation with fuzzy cognitive network. *IEEE Transactions on Energy Conversion*, 2006; 21(3).

[8] Aldobhani, A.M.S and John, R. Maximum power point tracking of PV system using ANFIS prediction and fuzzy logic tracking. International Multi Conference of Engineers and Computer Scientists, 2008.

[9] Iqbal, A., Abu-Rub, H., and Ahmed, S.M. Adaptive neuro-fuzzy inference system based maximum power point tracking of a solar pv module. IEEE International Energy Conference (ENERGYCON), 2010; 51-56.

[10] Shanthi, T. and Vanmukhil, A.S. ANFIS controller based MPPT control of photovoltaic generation system. *International Journal of Computer Applications*, 2013; 23-29.

[11] Tarek, B., Said, D. and Benbouzid, M.E.H. Maximum power point tracking control for photovoltaic system using adaptive neuro-fuzzy, ANFIS. IEEE Conference and Exhibition on Ecological Vehicles and Renewabel Energies (EVER), 2013.

[12] De Blas, M.A., Torres, J.L., Prieto, E., Garcia, A. Selecting a suitable model for characterizing photovoltaic devices. *Renewable Energy*, 2002; 25: 371-380.

[13] Chafle, S.R., and Vaidya, U.B. Incremental Conductance MPPT Technique for PV system. *Int. International Journal of Advanced Research in Electrical, Electronics and Instrumentation Engineering*, 2013; 2(6): 2719-2726.

[14] Saoud, M.S., Abbassi, H.A., Kermiche, S., Ouada, M. Improved incremental conductance method for maximum power point tracking using cuk converter. *WSEAS Transactions on. Power Systems,* 2013; 3(8): 124-133.

[15] Iqbal, A., Abu-Rb, H., Ahmed, Sk. M. Adaptive Neuro-fuzzy Inference System based Maximum Power Point Tracking of a Solar PV Module. IEEE International Energy Conference (ENERGYCON), 2010;51-56.

[16] Ahmed, B.H., Abdennour, A., Mashaly, H. An Accurate ANFIS-based MPPT for Solar PV System. *Int. J. of Advanced Computer Research;Bhopal*, 2014; 4(2): 588-595.

[17] Shanthi, T. and Vanmukil, A.S. ANFIS Controller based MPPT Control of Photovoltaic Generation System. *International Journal of Computer Applications*, 2013; 23-29.

[18] Wang, L. et al. Wind power systems, green energy and technology. *Springer-Verlag Berlin Heidelberg*, 2010: 255-295.

[19] Balaji Naik, M. and Sujatha, P. Adaptive fuzzy & neuro-fuzzy inference controller based MPPT for photovoltaic systems. *International Research Journal of Engineering and Technology*, 2015; 2(8): 693-701.